Numerical Simulation of the Aerosol Formation and Spreading in a Train Cabin

M. Konstantinov[1], D. Schmeling[2*] and C. Wagner[1,2]

[1]Institute of Thermodynamics and Fluid Mechanics, Technische Universität Ilmenau, Ilmenau, Germany
[2]Institute of Aerodynamics and Flow Technology, German Aerospace Center, Göttingen, Germany

Abstract

In this paper a numerical approach for the prediction of the unsteady aerosol formation and transmission process in a train cabin is presented. For that purposes models to simulate unsteady flows including the transient behaviour of two-phase atomization process and thermal air flow are employed. Results of aerosol distribution for coughing, speaking and breathing (with and without mask) in specified train cabin compartment are discussed. The dispersion of the exhaled droplets was analysed for a double cough, 10 s talking and continuous breathing of one source passenger. The results obtained show that the dispersion of aerosol particles in the cabin after coughing is two times deeper than when speaking, 2.5 times deeper than when free breathing and 17 times deeper than when breathing with a mask. Further, the results revealed that 2 minutes after the end of the coughing, only about 6% of active aerosol particles remain in the compartment and relatively clean air is again in the cabin.

[*]Corresponding author: Daniel.Schmeling@dlr.de
German Aerospace Center (DLR), Bunsenstraße 10, 37073 Göttingen, Germany

Keywords: aerosol dispersion, train compartment, computational fluid dynamics (CFD), thermal comfort model (TCM), cabin air flow, Lagrangian Multiphase Model.

1 Introduction

At the German Aerospace Center (DLR) the project Next Generation Train (NGT) addresses the question how the travel times of future trains can be reduced and at the same time how the safety, passenger comfort and environmental aspects can be improved (Konstantinov and Wagner, 2015). In connection with the risk of spreading of coronavirus SARS-CoV-2 the prediction of aerosol dispersion in train compartments became a major issue with regard to passenger safety and comfort.

A better understanding of the infection with the SARS-CoV-2 virus and in particular addressing the question of whether travelling on long-distance trains represents an increased risk of infection stands in focus of the Deutsche Bahn (DB) (Gravert et al., 2020). An overview of relevant Covid-19 infection risk publications in rail systems was presented at a rail industry forum (Rail Industry Coronavirus Forum, 2021). This paper indicated summarizes, that the coronavirus spreads through three main transmission routes:

- Contact transmission – between persons or via contaminated surfaces.
- Respiratory transmission – via small droplets (5-10 μm) carrying the virus.
- Respiratory transmission – via aerosol droplets (<5 μm) that remain in the air for some time.

A detailed report of the American Public Transportation Association (Chen et al., 2012) revealed, that ventilation and flow control reduced the risk of contact with and spread of respiratory droplets and aerosol.

Even if mean travel times in long-distance trains are still shorter than the mean passenger duration in an aircraft, the time-scales are comparable. Hence, looking at the aerosol dispersal and the reported infection transmissions in an aircraft is reasonable when addressing long-distance trains. The droplets exhaled by an index patient with infectious disease in an aircraft cabin have been investigated in detail in (Gupta et al., 2011) and in the report of the US Airliner Cabin Environment Research Program (Chen et al., 2012). In these works, the cases of coughing, speaking and breathing under typical aircraft ventilation conditions were experimentally and numerically investigated. In particular, for the numerical simulations monodisperse droplet sizes and concentrations were specified for different exhalation activities The investigation studied the transport of the expiratory droplets from an index patient seated at the centre of a seven-row, twin-aisle, fully occupied aircraft cabin. The droplets exhaled from the cough of the index patient followed mainly the bulk airflow. The droplet concentration in the vicinity of the passengers reduced over time due to the removal from the outlets and dispersion of the droplets. The total airborne droplet fraction reduced to 32% at 2 minutes and 12% at 4 minutes after the droplets entered the cabin. Most of the droplets were transported within one row of the index patient in the first 30 s and then distributed to the entire seven-row cabin with a uniform droplet distribution in 4 minutes.

Performing Computational Fluid Dynamics (CFD) simulations with CFD code FLUENT, the dispersion and deposition of the expiratory droplets were predicted in (Chao and Wan, 2006). The results indicate that characteristics of dispersion and deposition of expiratory droplets are highly dependent upon droplet size.

Droplet size distributions expelled during coughing and speaking and velocities of the expiration air jets of healthy volunteers were investigated in (Chao et al., 2009). The measured droplet size data were used for CFD simulations with the code FLUENT. The expiration air velocity was specified as 11.7 m/s for coughing and 3.9 m/s for speaking. The numerical results indicate droplet size distributions in two cross-sections 10 and 60 mm from the mouth opening as well as air temperature and air velocity distributions along a distance of 100 mm. A more detailed experimental analysis of the modality of expired aerosol size distributions for breathing, speech and coughing is given in (Jonson et al., 2011), showing a bi-modal size distribution.

In report of TRANSCOM/AMC (2020) experimental tracer aerosols were released from a simulated infected passenger, in multiple rows and seats in a Boeing 777 and in a Boeing 767 aircraft cabin, to determine the risk of exposure and penetration into breathing zones of nearby seats. One of their main findings was, that the penetration of aerosols occurs into the breathing zones of passengers seated in the same row and in numerous rows in front and back of the source.

In summary, the existing literature on aerosol spreading in aircraft cabins reveals that only rather low aerosol concentrations were found on the neighbouring seats, however, there is a non-zero dispersion of the aerosols within the seat row and on multiple rows forward and rear wards.

Considering the situation in trains again, the cough droplets dispersion processes inside three different train compartments were studies in CFD simulations to determine the droplets removal ability (Wang et al., 2014). Therein, the size of droplets generated by coughing is assumed to be 13.5 μm. However, boundary conditions regarding side walls and heat-releasing passenger dummies were not considered in detail. Strongly deviating ventilation efficiencies were found for the considered three Chinese train cabins, confirming the importance of the ventilation concept for an efficient removal of aerosols. The dispersion process of respiratory droplets released by coughing of an individual source in a high-speed rail compartment was studied in the CFD simulations of Zhang and Li (2012). The droplet distribution characteristics and the maximum distribution distances under specified ventilation conditions were considered in this study. The coughing individual is located on an aisle seat. The duration of a single cough was assumed to be 0.4 s and a time-dependent coughing velocity profile was prescribed. Within the first 10 s after coughing, a separation phenomenon of the so-called “old” and “new” droplets was observed. The “old” droplets generated in the first 0.2 s escaped from the body plume, and were injected into the lower zone of the cabin. These droplets remained longer in the lower zone of the compartment. The “new” droplets generated in the next 0.2 s, had a relatively small velocity, and thus followed the upward body plume, entering directly the upper zone.

In recent publications (Chong et al. 2021 and Ng et al. 2021) direct numerical simulations of a typical respiratory event are performed to quantify the fate of respiratory droplets. Their results on the evaporation process of the initial particle

cloud reveal that the lifetime of the smaller droplets with initial diameter d ≈ 10 μm gets extended by a factor of more than 30 times as compared to what was suggested with the classical model by Wells (1934) assuming a relative humidity of 50%. In the study of Ng et al. (2021) the initial distribution of the droplets was prescribed according to the distribution measured by Duguid (1946) for cough. A direct comparison was not possible because experimental data are taken after some time after cough, whereas numerical distribution was prescribed as initial conditions for DNS. The initial droplets were injected evenly in time with the same local inflow velocity of 11.2 m/s. Their results revealed that the droplets moved a distance of 0.8 m after 0.6 s of coughing.

Currently, by threat of infection connected with SarsCoV-2, the investigation of effects of protection mechanism of face mask is vitally important. Kähler and Hain (2020) experimental investigated the air flow fields from human probands by coughing and breathing with and without different medical masks. In agreement with other studies their results demonstrate, that the flow resistance of the mask greatly limits the spread of droplets and aerosols in the room.

Following the literature overview, it becomes apparent that there are only few studies which address the transient aerosol dispersion process in a train compartment, while on the other hand the strong differences of aerosol releasing events are highlighted. Accordingly, the aerosol propagation in a six-row long distance train segment passenger compartment is predict in a CFD transient simulation solving the Reynolds averaged Navier-Stokes (RANS) equation together with the k-omega SST turbulence model with Lagrangian Multiphase model. The cases of cough, speech and breath with

and without mask are investigated. The aim of our study is the spatial and temporal distribution of aerosol particles during coughing, speaking and breathing in train compartment under air ventilation conditions.

2 Numerical Method and Computational Details

The here considered aerosol transmission simulations are based on the solution of the Reynolds-averaged mass, momentum and heat transport equations in combination with the Lagrangian Multiphase Model of spray formation and atomization (Crowe et al. 1998).

The governing equations discussed below are discretized and integrated on a hybrid structured/unstructured mesh consisting of a total of 4 million cells and 4.5 million vertices which has been generated with the mesher of the commercial program StarCCM+. The grid covers the volume of a representative long-distance train segment with 6 rows and 24 passengers. This segment and the ventilation boundary conditions are presented in Fig 1. The cold air with T_{in} = 17°C propagates through the tiny hole channels in the ceiling. The outer temperature is 35°C. On the surfaces of walls and windows the corresponding wall heat transfer coefficients 1.2 W/m²K and 2 W/m²K are prescribed. The passenger temperatures were calculated with the Thermal Comfort Model (TCM) (see Konstantinov and Wagner, 2015). This model required that the passenger body persists of 14 separate segments. For all passengers in the train cabin, i.e. 14 x 24 = 336, separate body segment boundary conditions are specified. The calculations were started from well-developed steady state case. In Fig.

1 (a), the streamlines are color-coded with the velocity (upper legend), whereas all surfaces are color-coded with the temperature (lower legend). The main flow structure is represented by downward flow in the aisle (up to 0.4 m/s), flow towards the sidewalls in the leg room and rising flow along the warm windows and the heat releasing passenger manikins.

Two different source locations are simulated separately: P42 and P52, see Fig. 1 (b). Thereby, P52 is selected as a representative aisle seat for a face-to-back seat arrangement and P42 as an aisle seat at the table with a face-to-face configuration.

The following three variants of aerosol exhalation events are analysed: coughing, speaking and breathing. Thereby, the breathing case was considered with and without mask.

The simulations were performed with the StarCCM+ codes solving the transient weakly compressible Reynolds-averaged Navier-Stokes equations together the k-ω SST model using an unsteady implicit time integration scheme with a time step of $10^{-3}s$ and second order finite differences in space. To predict the droplet motion the Lagrangian Multiphase model was used, which solves the equation of motion for representative parcels of the dispersed phase as they pass through the continuous phase. Here, dispersed phases modelled using the Lagrangian Multiphase model are called as Lagrangian phases. The parcels in the Lagrangian model (Crowe et al., 1998) are known as particle-like elements that are followed through the continuum. The state of each parcel is updated according to a selected set of models and can be optionally recorded as a track. For the aerosol computations, the primary Linearized Instability Sheet Atomization (LISA) model (Schmidt et al., 1999), the break-up model of Reitz-

Diwakar (1987), NTC collisions model (Senecal et al., 1999) and wall-impingement model of Bai and Gosman (1995) have been used.

The Linearized Instability Sheet Atomization (LISA) model is a primary atomization model that represents the action of a pressure swirl atomizer. The model generates initial size and velocity values for droplets entering through hollow cone injectors active for the Lagrangian phase. The NTC collision model distinguishes between coalescence, separation and bouncing interactions. Bai-Gosman wall impingement model provides a methodology for modelling the behaviour of droplets impacting on a wall. In particular, this model attempts to predict how and when droplets break up or stick to the wall.

To compute the aerosol propagation the so-called two-way coupling model was used. For Lagrangian simulations, the two-way coupling model allows the particle phase to exchange mass, momentum, and energy with the continuous phase. With the Two-Way Coupling model, the reverse effect is accounted for, and Lagrangian source terms appear in continuous phase equations.

The realistic chemical conditions of particles and their evaporation was not considered, for simplification water was chosen as liquid phase. This is possible because the small aerosol particles have a relative long lifetime up to 10 - 30 min depending on air change per hour (Yang et al., 2011). In recent publications (Lohse, 2020 and Bourouiba, 2021) it was clarified that the cloud of smallest droplets reaches up to 8 meters and persists for up to 10 minutes. The neglect of evaporation is reasonable, since the exhaled aerosol droplets reach their final size within milliseconds (Morawska, 2006) and thus no further evaporation has to be considered.

a)

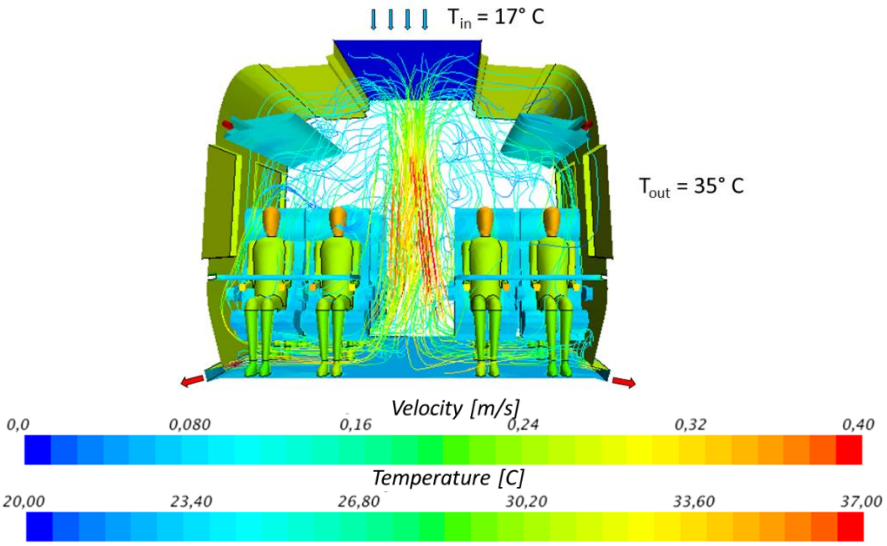

b)

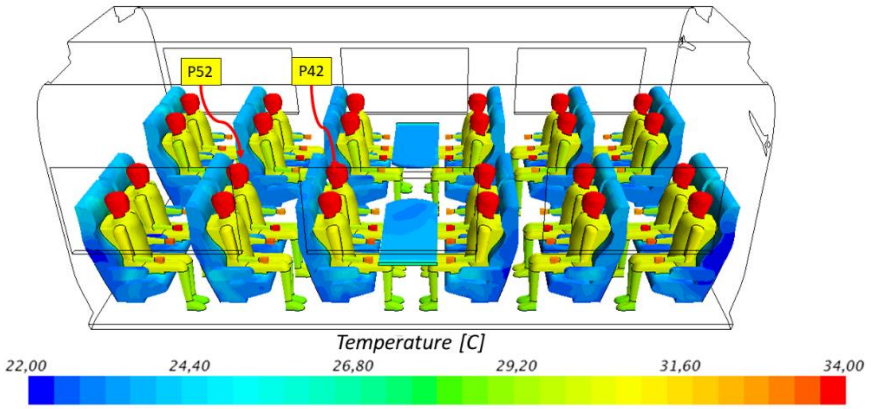

Figure 1: Streamlines and surface temperatures in a segment of the train cabin for summer conditions. Inflow (blue arrows) and outflow (red arrows) areas are additionally shown (a) and image of the 6-row, 24 seats numerical cabin segment for investigation with indication of test persons. The passengers, seats and tables are colored with surface temperatures (b).

The aerosol formation through a mouth or a nose is modelled as Hollow Cone Injector (see Fig. 2), which is situated at the passenger's head. A hollow cone injector injects parcels in a cone formation around a specified axis. An inner cone angle and an outer cone angle define the spray cone. The specified number of parcel streams are injected in random directions conforming to a uniform distribution on the surface of the cone. Given the direction, the velocity is obtained using the specified volume flow rate. The

direction and size distribution are randomized and newly sampled each time-step. An injector diameter defines the value of the injector hole through which the droplet fluid flows.

All types of transient aerosol dispersions were started from steady-state turbulent solution with heat transfer and radiation. We consider three general types of aerosol dispersion under summer ventilation case: coughing, speaking and breathing, whereas the injector positions for coughing and speaking are the same. The positions of injectors for the examined cases are shown in Fig. 2. For the case of free breathing with mask, an additional injector is defined (c).

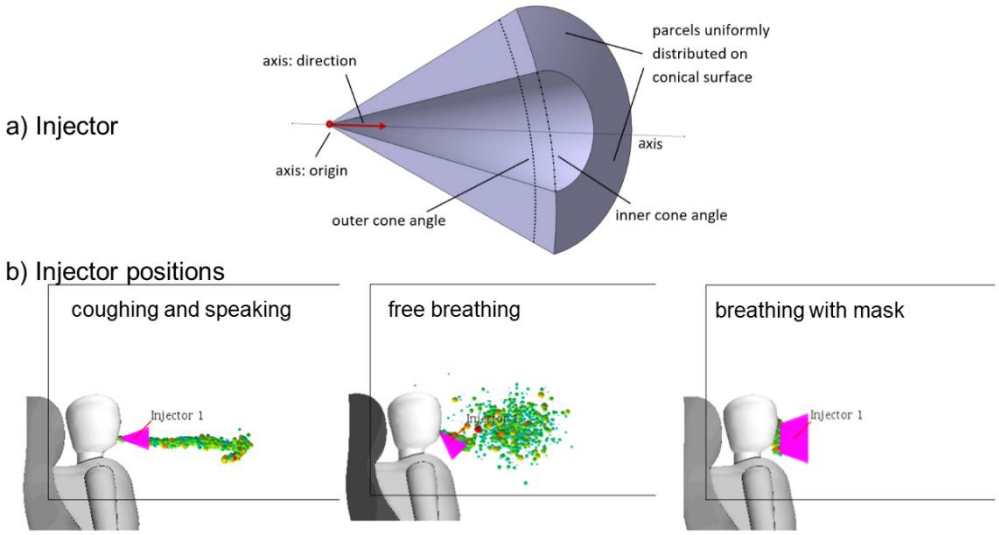

Figure 2: a) Scheme of Hollow Cone Injector, according to User Guide StarCCM+ (2014) and b) injectors positions for coughing and speaking, free breathing and breathing with mask.

The flow boundary conditions at the nose and mouth of the index passenger were different depending on whether he/she was coughing, breathing or talking. In the following, the boundary conditions and the exhalation jet direction for coughing, breathing and talking processes of the index passengers are specified. For rest the

passengers the mouth was assumed to be closed. In real situations all the passengers, including the index passenger will breath.

The flow rate generated from a typical cough over time from a subject was presented in Chen et al. (2012). The results indicate that the cough began with a very short inhalation (<1% of the total exhaled air volume), a very high acceleration afterwards in exhalation and subsequently a decay. The pre-cough inhalation volume was very small and may be neglected.

The temporal velocity distribution of the liquid phase during coughing was selected similarly to Chen et al. (2012). To enhance the effect of coughing, two coughs with interval 0.5 s were prescribed (see Fig. 3 (a)). The aerosol spreading after the cough event is calculated for 120 s. The nominal air exchange in the train compartment takes place in 150 s ((cabin volume) / (HVAC volume flow)), i.e. 24 air change rate per hour (ACH).

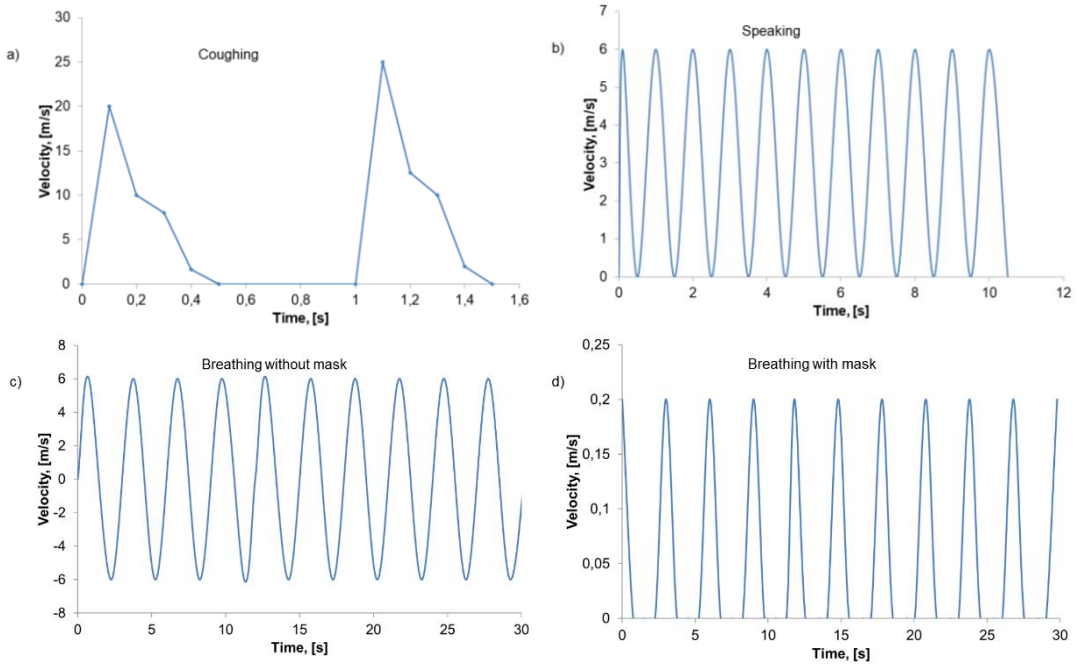

Figure 3: Transient air velocity at Hollow Cone Injector for the coughing (a), speaking (b), breathing without mask (c) and breathing with mask (d).

In the case of speaking, the air velocity distribution on the mouth boundary was chosen as depicted in Fig. 3 (b). It was assumed that a sentence consists of ten words of similar length. Consequently, the exhalation velocity oscillates between zero and 6 m/s. In this case, only the exhalation velocities were considered. Inhalation velocities were neglected. We observe the aerosol spreading during one sentence, i.e. 10 s of speaking, and one compulsive pause of 10 s.

The current investigation of aerosol behavior during breathing considers two situations: with and without a face mask. In contrast to coughing, a significantly lower liquid volume flow (0.002 ml vs. 0.625 ml) and droplet sizes are reported, see Table 1. For free breathing the direction axis of injector is aligned with an angle of -45° with respect to the horizontal axis. Thus, the breathing with the nose is modelled (see Fig 2b). The specified boundary air velocities at the nose for free breathing are presented in Fig. 3 (c). In this case, the inhalation and exhalation are modelled with a time period of 3 s.

The mask effect is modelled with considerably greater injector diameter (see Table 1) and consequently due to the same volume flow rate, smaller initial velocities (peak magnitude of the velocity 6 m/s vs. 0.2 m/s). The fluid filtration through the mask and separation efficiency of the particles were not considered. Only exhalation is considered, inhalation is ignored. The injector direction axis is normal to the head. The initial air velocities for breathing with mask are presented in Fig. 3 (d). Here, due to the higher effective exhalation area, the magnitude of the velocity reaches peak values of only 0.2 m/s.

For all considered cases, the transient volume rate of the liquid phase is given with corresponding time course. A total of 0.625 ml of liquid phase was injected for one cough, 0.01 ml for 10 s of speaking and 0.002 ml for one breath for both cases of breathing.

In the current investigation we have chosen the statistical distribution of Rosin-Rammler (Rosin and Rammler, 1933; Lefebvre, 1989). The Rosin-Rammler distribution was developed to describe the volume distribution of particles as a function of their diameter *F(D)*:

$$F(D) = 1 - \exp\left[-\left(\frac{D}{D_{ref}}\right)^{q}\right],$$

where D_{ref} is the Rosin-Rammler diameter and q is the Rosin-Rammler exponent.

For coughing, the reference droplet size was chosen 10 μm, for speaking 20 μm, for free breathing 1μm and for breathing with mask 0.5 μm. These sizes represent the values in agreement with the literature. However, there is a wide range of literature on expiratory droplet size and concentration measurements for coughing, breathing, and talking processes (Duguid, 1946; Yang et al., 2007 and Fabian et al., 2008). There were differences in the finding as these measurements were performed on different subjects using different methods. Yang et al., (2007) found that the average mode size of droplets exhaled during coughing was 8.35 μm.

Following the literature (Gravert et al., 2020 and Rail Industry Coronavirus Forum, 2021), the particle size for speaking is larger than for breathing. Moreover, the speech frequency is higher. In Gupta et al. (2011) and Chen et al. (2012) the uniform droplet

diameter size of 30 μm was specified. In Chao et al., 2009 the geometric mean diameter of droplets for speaking was 16 μm, while Duguid (1946) reported 30 μm. The droplet size for breathing is much smaller than for talking. Fabian et al., 2008 found that the droplets exhaled by the influenza infected subjects were mostly in the range of 0.3 to 0.5 μm. In Gupta et al. (2011) the uniform droplet size of 0.4 μm was used, while in paper of Johnson et al. (2011) the mean size of droplet by breathing is approximately 1 μm.

The injector data for all investigated cases are summarized in Table 1.

Table 1: Injector data for coughing, breathing and speaking.

Variant	Cough	Free Breath	Breath with Mask	Speech
Particle Diameter:				
Minimum, [m]	1.0e-6	1.0e-7	1.0e-7	1.0e-6
Maximum, [m]	1,0e-4	1.0e-5	5.0e-6	4.0e-4
Reference, [m]	1.0e-5	1.0e-6	5.0e-7	2.0e-5
Exponent	2.0	2.0	2.0	2.0
Injector Diameter, [m]	0.007	0.007	0.11	0.007
Inner Cone Angle, [rad]	0.5	0.5	0.5	0.5
Outer Cone Angle, [rad]	0.7	0.7	0.7	0.7
Temperature, [°C]	36.7	36.7	36.7	36.7
Volume Liquid [ml]	0.625/cough	0.002/breath	0.002/breath	0.01/10s

The velocity and volume flow rate of the liquid phase were specified with time-dependent tables at injector settings.

3 Discussion of Results

Fig. 4 reveals the calculated droplet size distribution after a cough and for speaking at the end of a sentence at 10 s in comparison with measured data of Duguid (1946), Chao et al. (2009) and Yang, S. et al. (2007). Here, N_p is the particle number and N_{pmax} denotes the highest value of N_p. After a cough, the calculated average droplet size is equal to 8.5 µm. This value corresponds to the average size mode of droplets exhaled during coughing found by Yang et al. (2007). The same droplet size of 8.5 µm was used in the calculations in Gupta et al. (2011) and Chen et al. (2012), but there all droplets had a uniform diameter. In numerical calculation for speaking in Gupta et al. (2011) the droplet size of 30 µm was used.

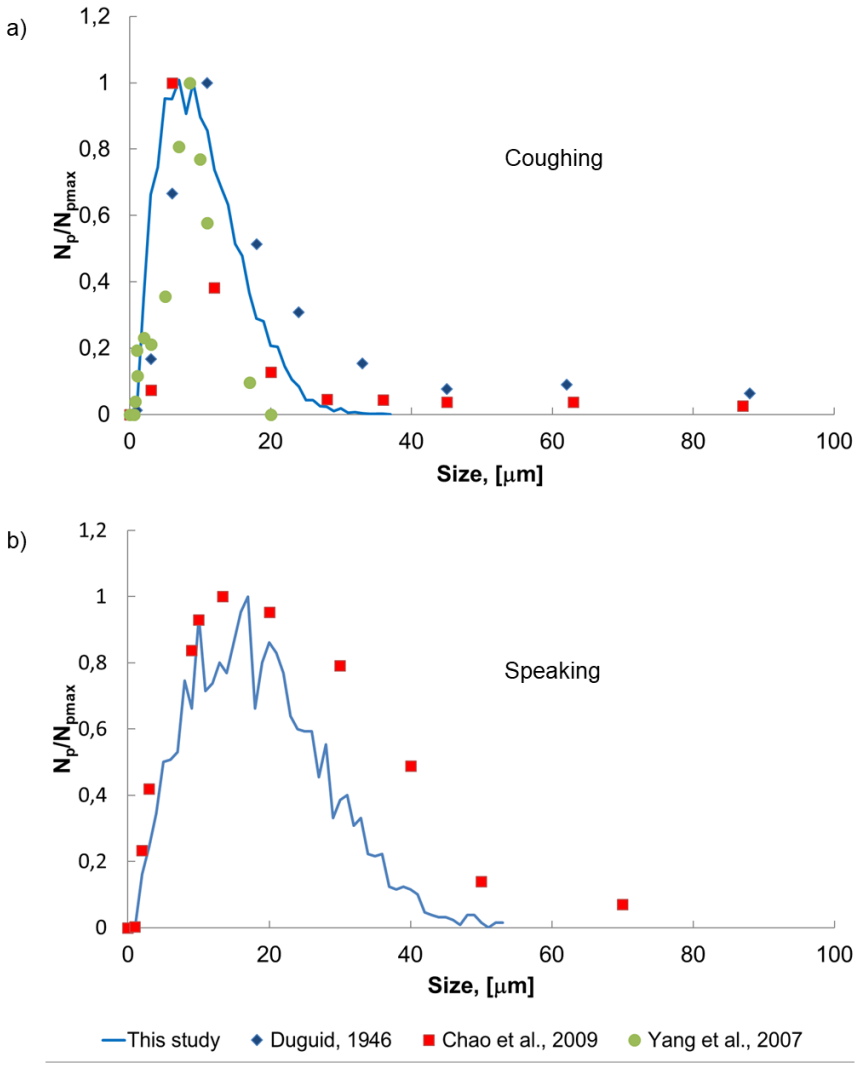

Figure 4: Calculated particle size distribution after one cough (a) and after a sentence at 10 s and experimental data of Duguid (1946), Chao et al. (2009) and Yang (2007).

Fabian et al. (2008) found that droplet sizes during normal breathing exhalation were in the range of 0.3 to 0.5 μm. In Johnson et al. (2011) the droplet sizes are measured in the range of 0.7 to 20 μm, whereas in Gupta et al. (2009) the constant size 0.4 μm was used for the calculations. Since no reliable droplet size distributions are currently known for the case exhalation with mask, we assumed a mean droplet size during exhalation with mask of 0.3 μm.

In our simulation the droplet size distributions shown Fig. 5 was predicted after exhalation.

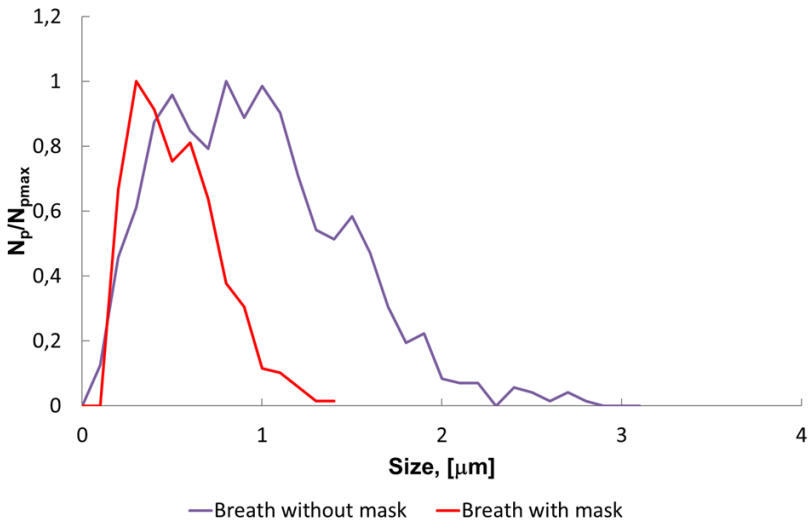

Figure 5: Calculated particle size distribution after an exhalation with and without mask.

The particle distributions after the start of emission for the four different considered generation processes are presented in Fig. 6. Additionally, the velocity field in the cross section of the manikin is depicted as background for three instants in time: 0.3 s, 1.5 s and 10 s (top to bottom). From left to right the series of images shows coughing, speaking, free breathing and breathing with a mask. As expected, the main differences are found comparing coughing with the other cases. Here, the high initial momentum of the particles results in a clearly visible jet of particles also influencing the flow field in the area in front of the manikin. For all other cases, only minor differences are found in the vicinity of the face of the source manikin. Thereby, the penetration depth of the aerosol jet decreases from speaking to free breathing and further to breathing with mask.

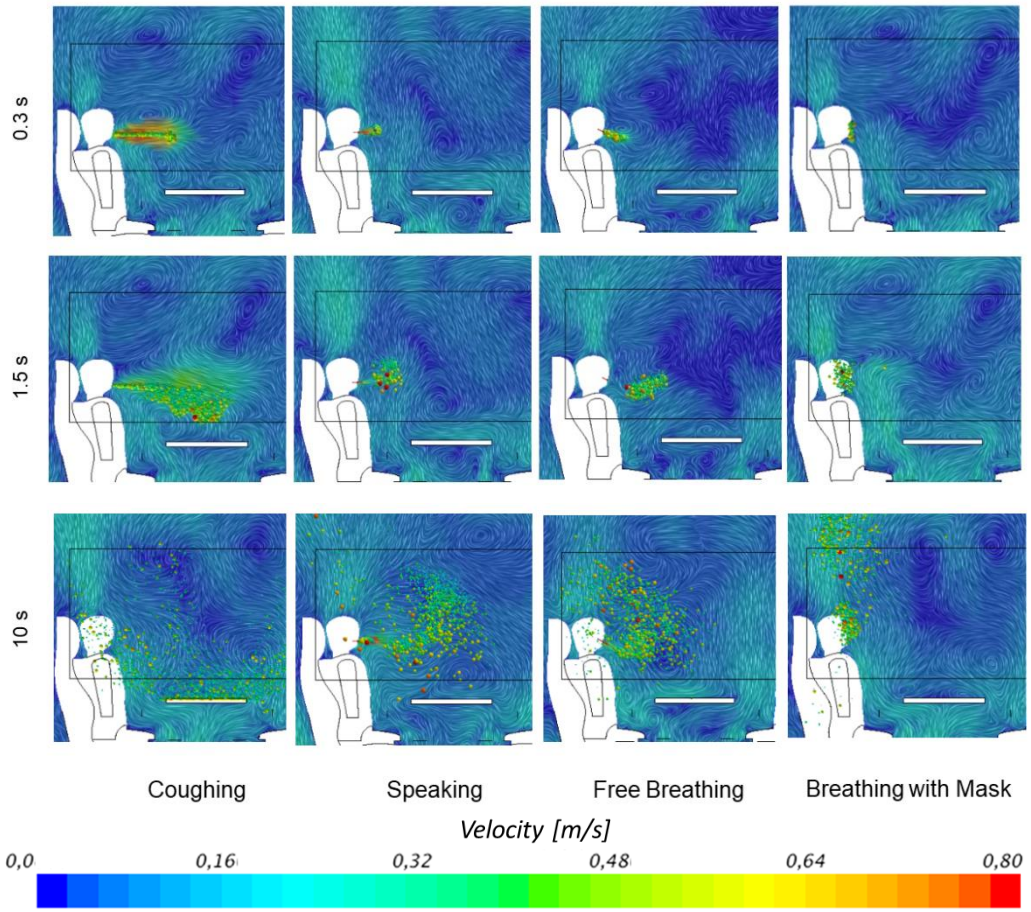

Figure 6: Characteristic particles behavior in the first 10 s for the considered cases (from left to right: coughing, speaking, free breathing and breathing with mask). The velocity distribution in the cross-section of the manikin is shown, superimposed with the particles within and in front of this cross-section only.

The calculated behavior of aerosol cloud dispersion in the initial phase develops similarly to results obtained in experimental boxes without additional ventilation (see e.g. Scharfman et al., 2016; Kähler and Hain, 2020; Hassan et al., 2022).

At the beginning, almost all droplets move in one direction. Later, the directions of movement are divided. The smaller lighter and warmer droplets will gradually rise and the larger ones will fall down. In the further time, the dispersion of the droplets becomes dependent on convective airflow in the train segment.

Fig. 7 shows the time-dependent length of aerosol propagation in the train compartment for all cases up to 20 s. The results show that the dispersion of aerosol particles in the compartment is significantly faster and deeper for coughing in contrast to talking and breathing. In the first 10 s, the particle cloud reaches a distance of 1.7 m when coughing. For speaking and breathing, the aerosol particles spread out during the same time for only approx. 0.7 m. For breathing with a mask, this distance is 0.1 m.

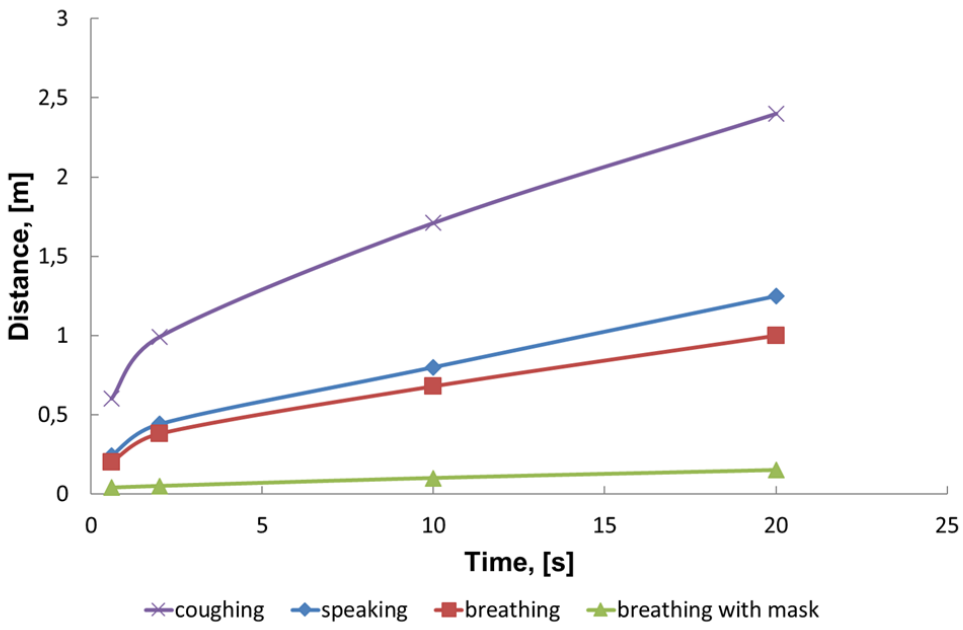

Figure 7: The horizontal length expansion of the droplet cloud as a function of time up to 20 s. In both breathing cases, the continuous injection of droplets occurs; in the case of speaking, only one sentence is uttered within 10 s, and in the case of coughing, two coughs were uttered within 1.5 s.

Further (after about 20 s), the droplets fly with convection flows also in cross and back directions. Note that here the results for continuous breathing are considered in contrast to coughing (double cough within 1.5 s) and speaking (one sentence within

10 s). These results show that a distance of 1.5 m between passengers is not sufficient for coughing.

3.1. Flow Analysis of Coughing

The dispersion of liquid particles after the coughing event were examined for two source locations, firstly the infected person was passenger P42 and at the secondly P52, see Figure 1 (b).

Due to gravity and the ventilation in the compartment, the number of "active", i.e. still flying in the compartment, particles reduced with time. The relative number of active droplets which are still in the compartment are presented in Fig. 8 for the two source locations. Here, additionally the curves for the fractions of particles that are smaller than 6 μm are shown in red. The graph reveals that after 20 s only about 40% of the initial number of aerosols are still active in the compartment, continuously falling to values around 5% after 120 s.

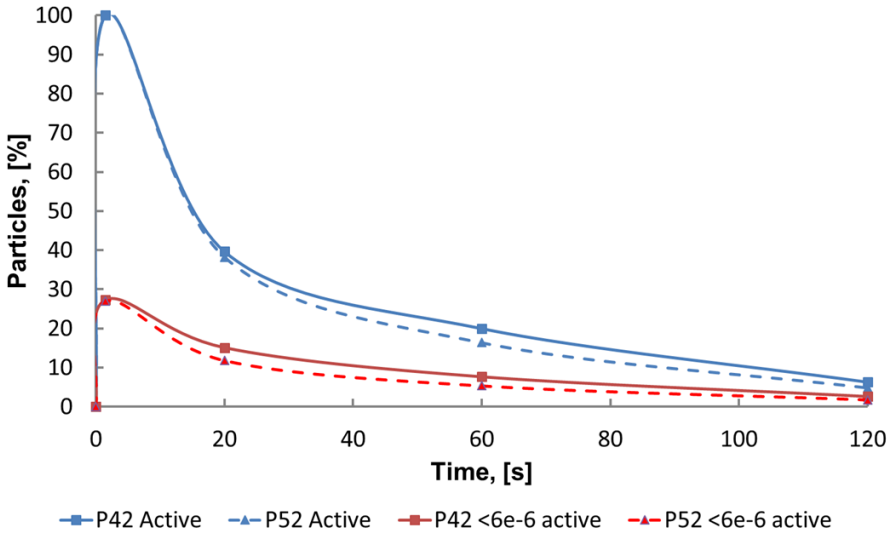

Figure 8: Time diagram of active droplet size distribution for seats P42 and P52.

Following the diagram with the time dependency of the active particles after a double-cough event, the table 2 summarizes the calculated parameters. Herein, the numbers of active (total and <6 µm), removed (by the air flow) and stuck, i.e. to surface attached particles, are given for different points in time. The data reveals, that in case of P42 considerably more droplets remain stuck on the walls compared to case P52. This is caused by the fact, that more particles are allocated on the surface of the table (P42) compared to the back of the seat in front (P52). Simultaneously, significantly more droplets have been removed from the compartment in the case P52. The largest differences between the two source positions were found at 60 s after the coughing event: here approx. 20% of the initial particles are still active for P42, whereas only 16% are still active for P52. After 120 s this difference decreases, here 6% and 5% of remaining active particles are found for P42 and P52, respectively. A deeper look at the smaller particles, i.e. < 6 µm, revealed that after 60 s, 28% of the initial small

particles are still active for P42, whereas for P52 only 20% are found. After 120 s these values go down to values as low as 10% and 7% for the both source positions.

Table 2: Droplets number at different time for P42 and P52.

Time, [s]	1.5		20		60		120	
Case	P42	P52	P42	P52	P42	P52	P42	P52
Active	9838	9849	3903	3763	1968	1612	622	477
Remote	0	0	1	1919	247	2245	482	2449
Stuck	0	4	5934	4179	7623	5996	8734	6927
$d < 6\ \mu m$	2683	2660	1485	1165	756	528	261	176

Aerosol propagation by coughing for passengers P42 and P52 at different moment of time are presented in Fig. 9. In the both cases intense particles-wall interaction is observed. Dependent on the particles' kinetic energy, the rebound, splash or stick of droplets on the wall surface occurs. The large and weighty droplets sink down, the smaller (up to 6 μm) rose firstly in the cabin and then are shifted with air flow field. The table in front of place P42 prevents droplets movement downwards. This slows down the removing the droplets from the cabin. In the case of P52 the splashing of droplets on the back of the front seat was observed. The similarly phenomenon occurs in the aircraft cabin too (Yan et al., 2020). In case P42 the particles move in table direction. Some of these particles later stuck to the table surface. In the other case P52, the particles tread the back seat. Part of the particles is reflected by the seat surface, another part sticks to it. During further aerosol dispersion, the particles with low kinetic energy stick to other solid surfaces (walls, windows, floor, etc.). Even if this

part of the aerosol is not actively distributing in the compartment anymore, and thus cannot be inhaled by other passengers, the potentially contaminated surfaces will need a cleaning depending on the survival times of the viruses attached to surfaces. The latter is strongly depending on the material properties and also under deep scientific investigation (Casanova et al., 2010), however, not in the scope of the present manuscript.

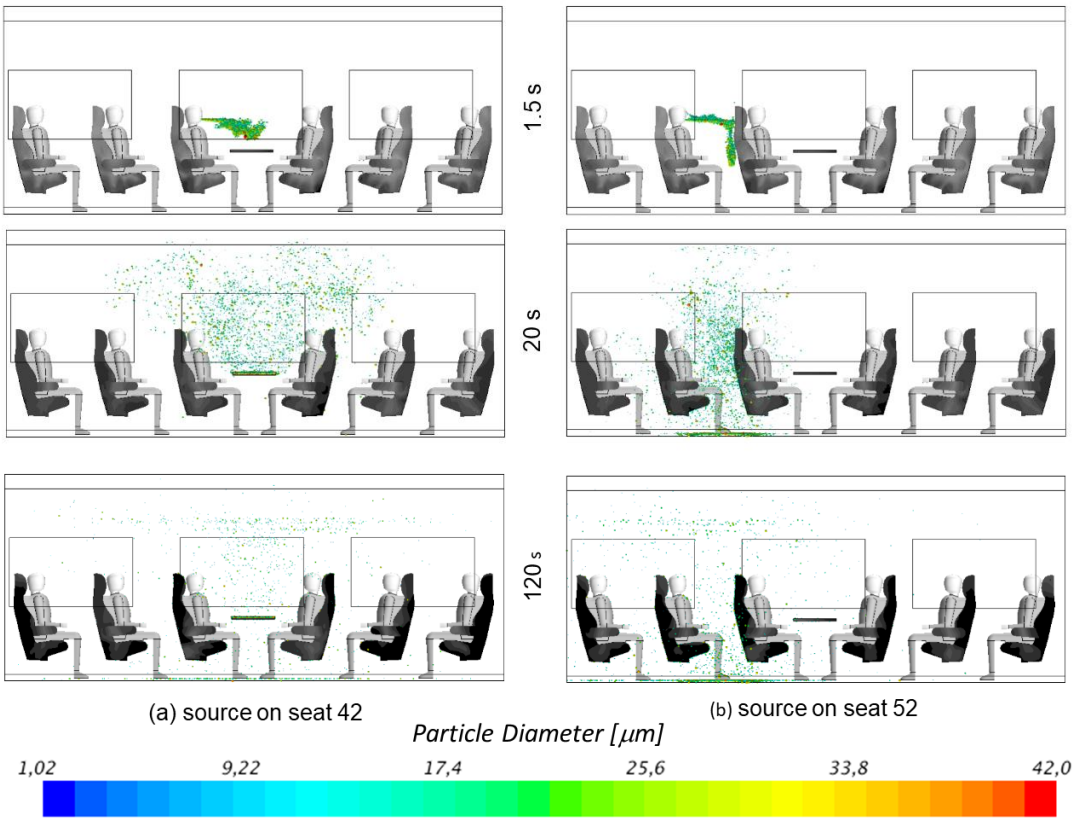

Figure 9: Time-development of aerosol dispersion for coughing from source location P42 (a) and source location P52 (b). Supplemental movies available online.

After the initial momentum of the aerosol particles has degraded due to friction, the total process of droplets motion can be explained with the behavior of the velocity fields in Fig. 10. Here two cross-sections near to passengers P42 and P52 are shown. In these sections two mutual vortices prevail, which retrieve the small particles. First,

the light droplets rise by convective flow towards window seat, and then they are pushed down in the aisle area.

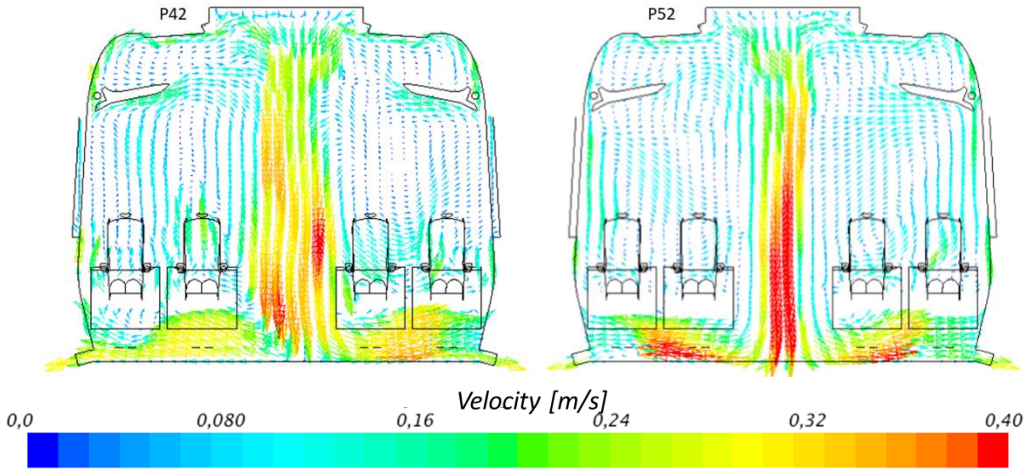

Figure 10: Air velocity fields (color coded magnitude) in two different cross sections in front of seat P42 (left) and P52 (right).

After this discussion on the aerosol droplet propagation for coughing in the train compartment, we will briefly analyze two possible infection paths: firstly, the airborne transmission and secondly the smear transmission. Both paths are only addressed in the sense of the liquid volume evaluation. Real inhalation and smear infection via other surfaces than the passengers' heads are not considered. Following these assumptions, the integrated concentrations on head levels are utmost importance. The dispersion of the liquid phase volume relative to the total exhaled liquid in % in the horizontal cross-section at the level of the mouth is shown in Fig. 11. Immediately after the end of the double cough at t = 1.5 s, the higher concentration values of cough-introduced liquid volume in the core of the stream are observed. Shortly later, at t = 20 s, the peak values of liquid volume fraction already disappeared completely, therefore, lower concentrations are found in the free space in front of the source. In

order to better understand the distribution of the liquid concentration in the cross-section, two different color scales were used. For t = 1.5 s in the zoom windows a scaling of 0.001 to 2 % was chosen, the main scaling for whole set is between 0.001 and 0.02%. The relative volumes that are below this value were not considered. For source position P42, the liquid is additionally transported towards the windows above the tables. In the case of the P52, the particles first move downwards, thus reduced the liquid area in cross-section at t = 10 s. Then the lighter particles rise upwards with air vortex flow (see Fig. 10). Therefore, at t = 20 s the liquid concentration in this cross-section increases again. Finally, at t = 120 s, the liquid concentration in the train compartment is significantly reduced.

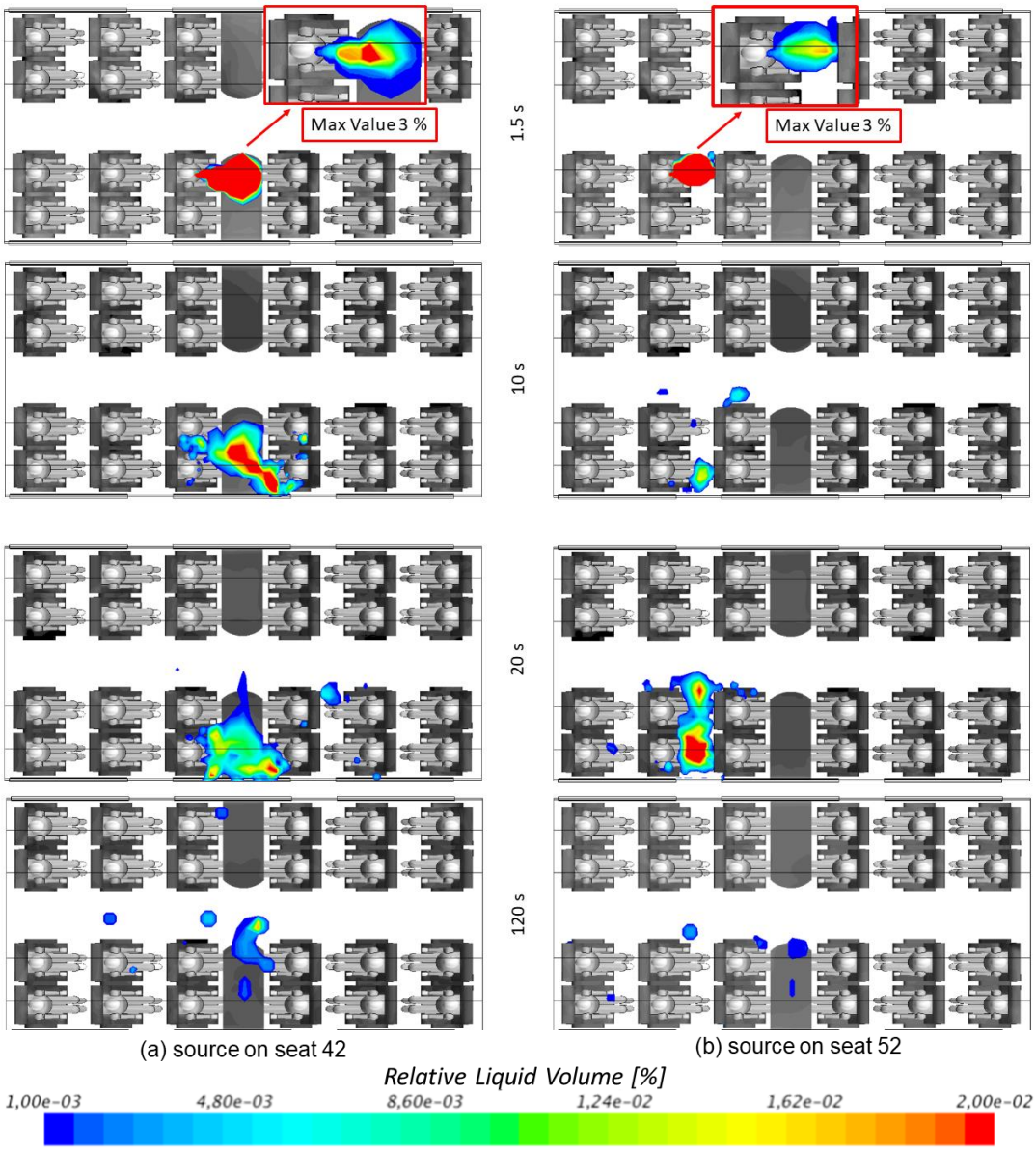

Figure 11: Relative liquid volume concentration to total exhaled liquid in % in the horizontal cross-section on the mouth level for coughing: (left) source on seat 42 and (right) source on seat 52. Top to bottom: time development. At time 1.5 s in zoom window, the distribution is displayed with scaling from 0.001 to 2%. The maximum values in some cells at this time are up to 3%.

After the presentation of time-development dispersion of the airborne relative liquid volume, we evaluate the number of droplets stuck on the face of the passengers for a total time of 120 s.

The relative count of droplets adhering to the passenger's face surface in % to total number of droplets sprayed into the train compartment by the emitters on seat P42 and seat P52 is shown in Fig. 12.

For case P42, the highest value (0.2 %) was determined for the passenger diagonal on the other side of the table (P31). The two other passengers P32 and P41, also sitting around the table, reveal the next highest amounts of adhered droplets to the heads. Further non-zero values were found for passengers P12, P21 and P52. The passengers whose heads look "grey" in Fig. 12 are not affected by droplets adhered to their heads. In the case of emitter P52 the peak value is found on the direct neighbor P51 (0.06%) is more than three times lower than the peak values found for source P42. Second highest value is detected for the passenger in front of the source (P42). However, there are six more seats with non-zero values of adhered droplets at the passenger heads.

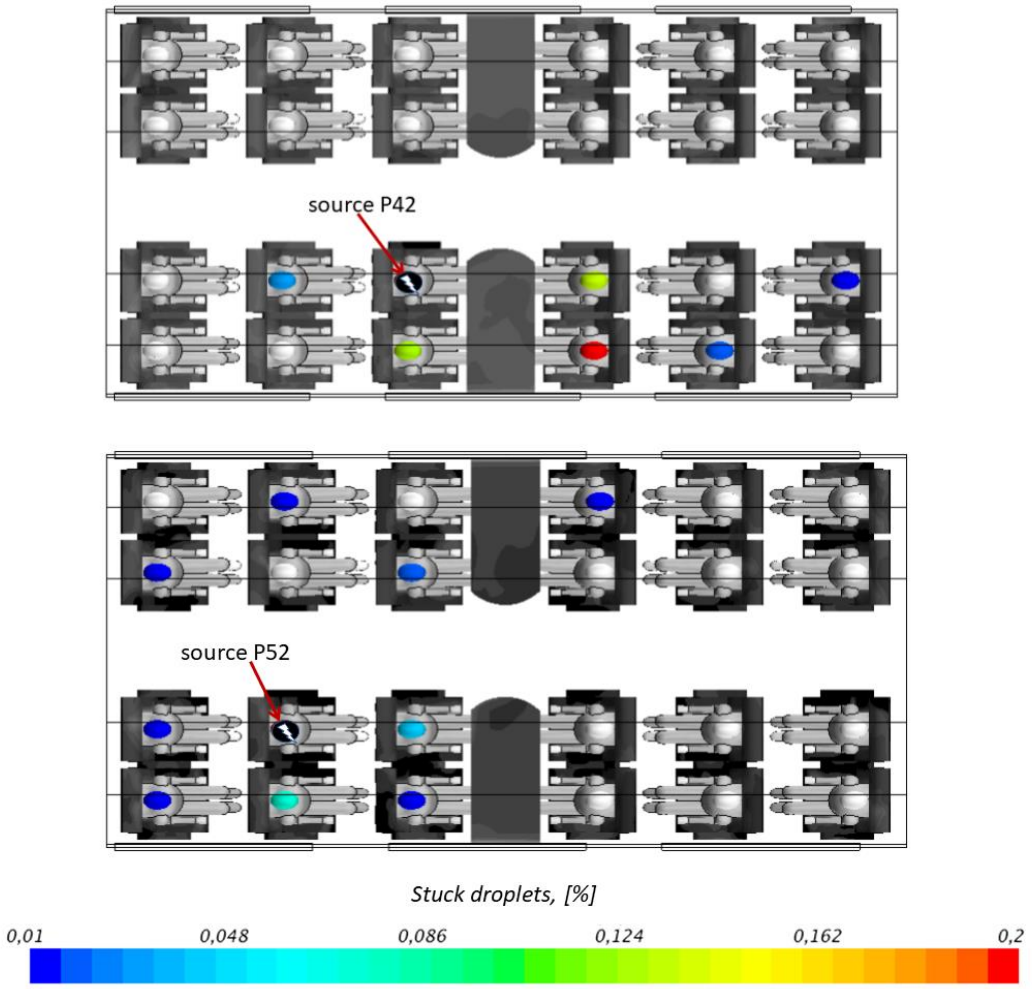

Figure 12: Relative number of droplets adhering to the passenger's face surface in % to the total number of droplets after double coughing by the emitter on seat P42 (top) and on seat P52 (bottom). The highest value by passenger: P31 (0.2 %) on emitter P42.

The results show that the liquid concentration on the neighboring persons in case P42 is 3 times higher compared to case P52.

Closing this brief discussion of the possible contamination paths, we want to emphasize, that we are fully aware, that the presented evaluations represent neither the really inhaled aerosols nor the total smear infection path. Accordingly, a quantitative evaluation of total incorporated aerosols or even an infection risk is not feasible. However, the analysis of the relative liquid volume dispersal, regarding both

airborne transmission and face covered surface are reasonable indicators for the possible transport of exhaled viruses to other passengers.

3.2. Flow Analysis of Speaking

Fig. 13 presents the aerosol distribution within the train compartment when one person (P42 at the table) is speaking. The figure shows the initial process of particle generation during this one sentence. At the end of the sentence (i.e. after 10 s), no more particles are generated and the first particles have travelled about half the distance to the passenger on the opposite side of the table. After 20 s the particles have already reached the opposing passenger and are distributed above the table.

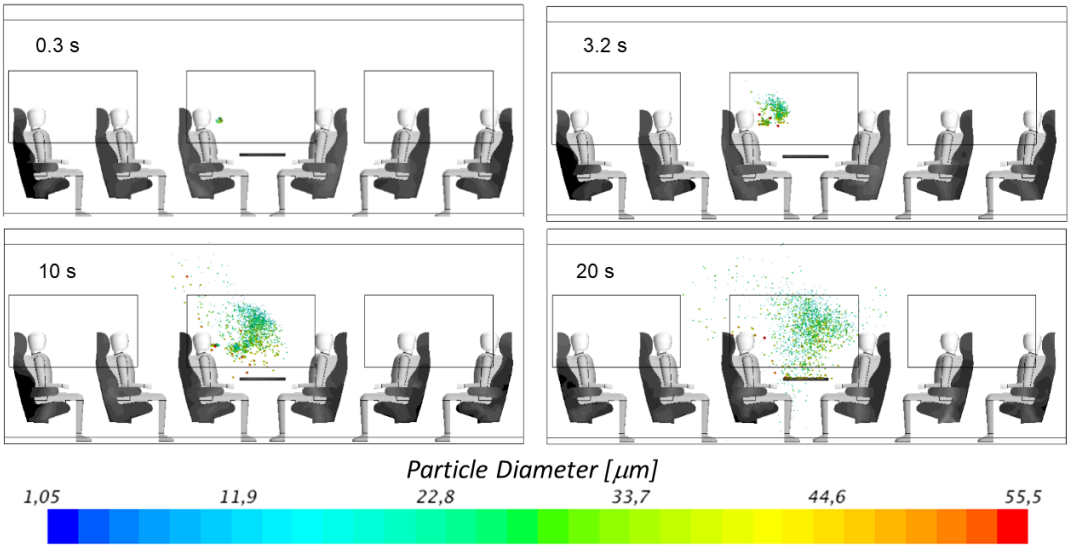

Figure 13: Particle behavior during and after the speaking. The diameter of the particles is color-coded. Supplemental movie available online.

The corresponding relative liquid volume concentration with regard to the total exhaled volume (see Table 1) in a horizontal plane at mouth level is shown in Fig. 14.

As discussed with the previous picture, after one sentence, the volume of liquid is mainly concentrated in a "cloud" above the table. After about another 10 s, i.e. 10 s after the end of the sentence, the opposite passenger is reached by the exhaled liquid. Here it should be noted, that the concentration of liquid phase 10 s after speech (t = 20 s) is already as small as the liquid volume concentration 120 s after a cough event. This illustrates the much higher amount of fluid released during a cough event compared to “normal” speaking, which differs by a factor of about 100 for a double cough vs. 10 s speaking. In contrast to the double cough with aerosol initiation of 1.5 s, the aerosol injection for speaking takes 10 s.

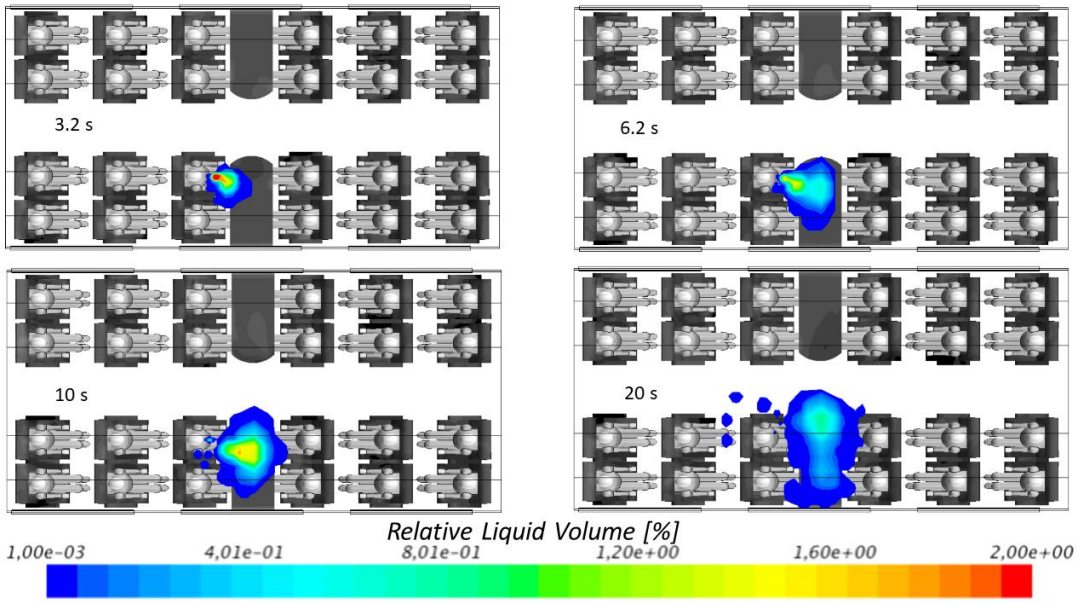

Figure 14: Relative liquid volume concentration to total exhaled liquid in % in horizontal cross-section on the mouth level for speaking.

Similar to the coughing case, we evaluated the total number of droplets sticking on the face of the passengers for the case speaking (without mask) after 20 s. Within the limitations of the evaluation procedure discussed above, we only found a non-zero value in the face area for the passenger opposite (0.03% to total number injected

droplets) all other passengers did not receive any particles stuck to their heads. For the sake of brevity and the limited additional information of a graphical representation of this finding, we did not show the corresponding figure here.

3.3. Flow Analysis of Breathing

At the edge of duct (modelling the nose openings) the transient air velocity is defined as shown in Fig. 3. During exhalation the particle cloud is formed and slowly separating from the emitter. During the following inhalation phase the particles closest to the emitter are slightly attracted due to the effect of the inhalation on the air flow in the compartment. However, this effect is small and only those particles which are still close to the emitter are affected. In the second exhalation phase a new particle cloud is produced which connects to the former one and forms an elongated area with increased aerosol concentrations. Afterwards, the effect of the flow field within the compartment on the particle movement starts do dominate and the initially produced particles lost all their initial momentum and start to move upwards.

The dispersion in the full compartment for two instants in time and for breathing with and without mask is presented in Fig. 15.In the case of breathing, no large droplets form as in the case of coughing and talking. Thus, the effect of gravity is smaller and there is no droplet movement downwards immediately after exhaling. The droplets first rise upwards and then move downwards with air convection flow in the aisle area. This effect is much stronger for breathing with mask (b) compared to free breathing (a). For the latter, the initial momentum of the exhalation through the nose forces the

particles downwards at first. Further, for breathing with mask, the particles are directly kept in the thermal plume of the heat releasing passenger and thus transported upwards faster. Afterwards, they move downwards due to the air flow in the aisle of the compartment.

In the case of breathing with a mask, hardly any forward movement is observed, see Fig 15 b. where almost no particles reach the are vertically above the table. Here, the light particles move upwards, which was also observed in experiments by Kähler and Hain (2020). Without a mask, the sideways turbulent flow that occurs during exhalation also transports the emitted aerosols forward.

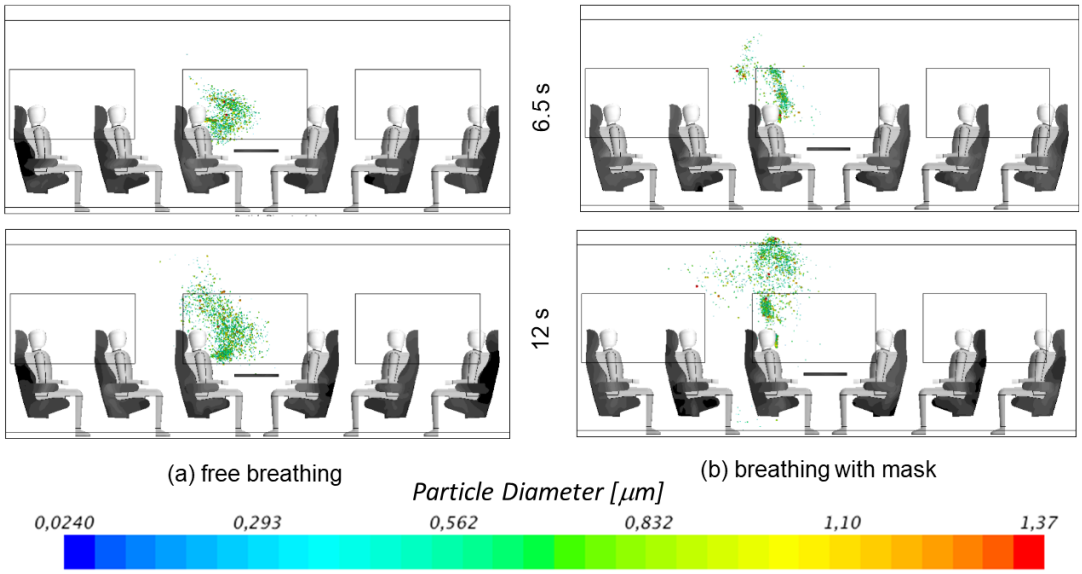

Figure 15: Comparison of particles spreading for free breathing (a) and breathing with a mask (b). Top and bottom, two instants in time (6.5 s and 12 s). The diameter of the particles is color coded. Supplemental movie available online.

In the case with the mask the first particles arrive at the exhaust openings already after 12 s. From 20 s, the continuous removal of the liquid droplets from the cabin begins. In the case of free breathing, the continuous removal of the liquid particles starts from 25 s. The distribution of particle velocities in this developed phase of continuous

droplet removal is shown in Fig. 16. In both cases, particle removal is observed through both outlet surfaces. By breathing with a mask, the droplets are transferred exclusively with convective airflow first upwards and then downwards in the aisle area. When breathing without a mask, the particles have a higher kinetic energy, move deeper into the cabin and later come to a quasi-equilibrium state.

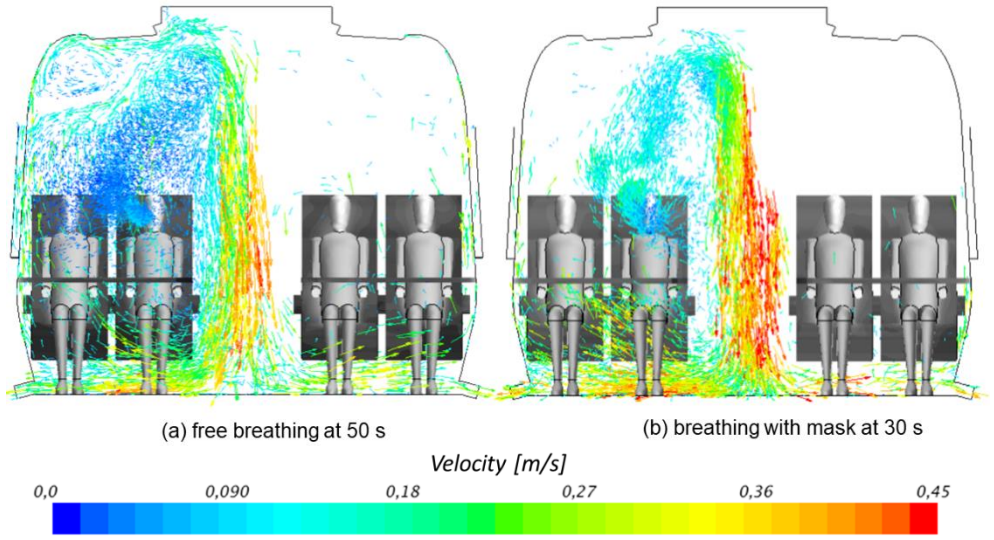

Figure 16: Vector representation of the particles velocities at quasi equilibrium state for both breathing cases, (a) without and (b) with mask.

The behavior of relative liquid concentration in cross-section on a height of 1.1 m, i.e. the breathing zone of the sitting passengers, is plotted in Fig. 17 for five instants in time. The first thing to note is, that for breathing with mask the amount of liquid remains directly at the emitter for the first seconds. Afterwards, it follows the thermal plume upwards and then the forced ventilation downwards in the aisle region (see also Fig. 16 b), resulting in slightly increased concentrations of the liquid phase in the aisle region after 20 s, see forth images of Fig. 17 b. Here values up to 0.1 % of the exhaled liquid volume are found in the aisle. For the free breathing a slightly enhanced

transport towards the neighboring passenger is found, this becomes evident in the time series of the relative liquid volume shown in Fig. 17 a. where the cloud containing the liquid volume reaches the neighbor on the window seat.

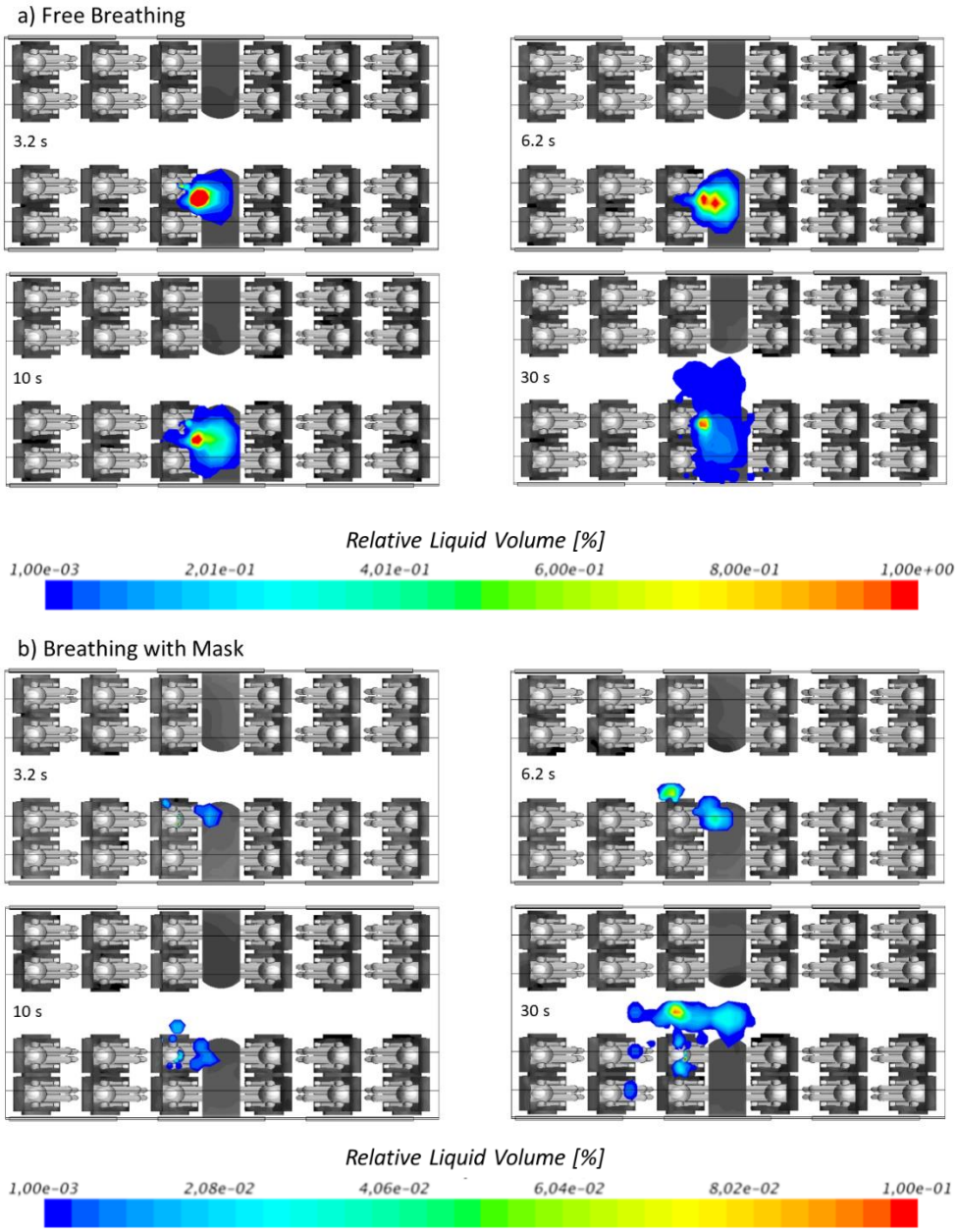

Figure 17: Relative liquid volume to total exhaled liquid in % in horizontal cross-section on the mouth level for two instants in time and both breathing cases: (a) without and (b) with mask. For free breathing, the maximum value of color scale is 1%, and for breathing with mask 0.1%.

The analysis of the results revealed, that wearing the mask is effective in preventing the aerosol spreading in horizontal direction. In the case of the mask, the smaller and lighter particles compared to free breathing (see Fig. 5) are first transported upwards by the convective flow and later move downwards towards the exhaust openings in the compartment. The main reason is the decreased exhalation velocity due to the dense membrane of the mask. At this point, it should be noted, that we assumed perfect masks with no leakage flows. It is well known, that this assumption does not hold when real passengers wear simple surgical masks. During breathing no droplets on the face surface of other passengers were found. Furthermore, our simulations assume that all passengers are seated. The possible movement of passengers in the cabin could lead to an enhanced aerosol dispersion during free breathing.

4 Conclusions

The presented numerical aerosol spreading predictions are based on the solutions of the URANS equation using a Multiphase Lagrangian Model and thermal comfort modelling for passengers. The applied simulation approach allows to predict the particles spread in the train compartment for coughing, speaking and breathing. Regarding the latter, two variants of breathing are investigated: free breathing and breathing with mask. Aerosol dispersion occurs in the train compartment under normal ventilation conditions. The results obtained show that the spread of aerosol particles in the cabin after coughing is two times faster and deeper than when speaking, 2.5 times faster and deeper than when free breathing and 17 times faster

deeper than when breathing with a mask. In detail, in the first 10 s, the particle cloud reaches a distance of 1.7 m when coughing. For speaking and breathing, the aerosol particles spread out during the same time for only 0.8 m and for free breathing for 0.7 m. For breathing with a mask, this distance is 0.1 m.

The evaluation of the results showed that during coughing, the total percentage of liquid droplets decreases to 6 % after 2 minutes and relatively clean air is again in the cabin. However, during this time parts of the exhaled aerosols reached also the breathing zone of other passengers. The low concentrations of aerosol particles disperse in the full compartment, i.e. the full 6-row simulation area. The highest values were found for a face-to-face configuration with a table for the person sitting diagonally opposite to the source. In contrast to coughing, free breathing and speaking lead to a significantly lower aerosol dispersion in the cabin, but other passengers could still be easily affected. The results obtained show that the dispersion of aerosol particles in the cabin after coughing is two times deeper than when speaking, 2.5 times deeper than when free breathing and 17 times deeper than when breathing with a mask. The higher initial momentum of the particles during speaking compared to free breathing reveals that the aerosol can reach the passenger sitting opposite. As a consequence, the passenger on the opposite side of the table is still slightly within the aerosol cloud, whereas for free breathing only the direct neighbouring seats could be affected. Comparison of breathing without and with mask points to important differences in aerosol dispersion in these cases. Looking at the effect of the mask during breathing, the presented work demonstrates clearly that the employment of a

mask leads to low concentration of liquid particles, which predominantly rise above the test person's head and hardly show any forward movement.

Acknowledgements

The authors would like to thank Mr. Felix Werner for the set-up of the CAD model and Dr. Andrei Shishkin for discussions on the numerical simulation of the aerosol dispersion analysis. Furthermore, we would like to thank the team of DB Systemtechnik for technical discussions within the scope of the current research exchange.

Funding

The study was funded by the German Aerospace Center (DLR).

References

Bai, C., & Gosman, A. D. (1995). Development of methodology for spray impingement simulation. *SAE Technical Papers 950283*.

Bourouiba, L. (2021). The fluid dynamics of disease transmission. *Annual Review of Fluid Mechanics, **53***, 473-508.

Casanova, L., Jeon, S., Putala, W., Weber, D., & Sobsey, M. (2010). Effects of air temperature and relative humidity on coronavirus survival on surfaces. *ASM Journals/ Appl. & Environmental Microbiology, 76, N9.*

Chao, C. Y. H., & Wan, M. P. (2006). A study of the dispersion of expiratory aerosols in unidirectional downward and celling-return type airflows using a multiphase approach. *Indoor Air **16**,* 296-312.

Chao, C. Y. H., Wan, M. P., Morawska, L., Johnson, G. R., Ristovski, Z. D., Hargreaves, M., Mengersen, K., Corbett, S., Li, Y. Xie, X., & Katoshevski, D. (2009). Characterization of expiration air jets and droplet size distributions immediately at the mouth opening, *Journal of Aerosol Science **40*** 122–133. https:// doi: 10.1016/j.jaerosci.2008.10.003.

Chen, Q., McDevitt, J. J., Gupta, J. K., Jones, B. W., Mazumdar, S., Poussou S. B., & Spengler, J. D. (2012). Infectious Disease Transmission in Airliner Cabins. National Air Transportation Center of Excellence for Research in the Intermodal Transport Environment (RITE) Airliner Cabin Environment Research Program Harvard School of Public Health; Kansas State University; and Purdue University, Report No. RITE-ACER-CoE-2012-01.

Chong, K. L., Shen Ng, C., Hori, N., Yang, R., Verzicco, R., & Lohse, D. (2021). Extended Lifetime of Respiratory Droplets in a Turbulent Vapor Puff and Its Implications on Airborne Disease Transmission. *Physical Review Letters **126**, 034502*

Crowe, C.T., Sommerfeld, M., and Tsuji, Y. (1998). Multiphase Flows with Droplets and Particles. *CRC Press, Boca Raton.*

Duguid, J.P. (1946). The size and the duration of air-carriage of respiratory droplets and droplet-nuclei. *Journal of Hygiene, **44***, 471-479.

Fabian, P., McDevitt, J.J., DeHaan. W.H., Fung, R.O.P., Cowling, B.J., Chan, K.H., Leung, G.M. and Milton, D.K. (2008). Influenza Virus in Human Exhaled Breath. *An Observational Study. PLoS ONE, 3(7), e2691.*

Gravert, C., Nagl, P., Ball, F., & Körner, T. (2020). Update on SARS-CoV-2 Infection Risks in Long-distance Trains. *Deutsche Bahn, Working Paper, September 2020.*

Gupta, J., Lin, C.-H., & Chen, Q. (2011). Transport of expiratory droplets in an aircraft cabin. *Indoor Air, 21(1),* 3-11.

Hassan, M. E., Hassan, A., Bukharin, N., Otaibi, H. A., Mofijur, M., Sakout, A. (2022). A Review on the Transmission of COVID-19 Based on Cough/Sneeze/breath Flows. *Eur. Phys. J. Plus, 137:1*, doi 10.1140/epjp/s13360-02162-9.

Johnson, G. R., Morawska, L., Ristovski, Z. D., Hargreaves, M., Mengersen, K., Chao, M. P., Wan, C. Y. H., Li, Y., Xie, X., Katoshevski, D., & Corbett, S. (2011). Modality of human expired aerosol size distributions. *Journal of Aerosol Science **42*** 839–851.

Kähler, C. J., & Hain, R. (2020). Fundamental protective mechanisms of face masks against droplet infections. *Aerosol Science **148** 105617.*

Konstantinov, M., & Wagner, C. (2015). Numerical Simulation of the Thermal Comfort in a Train Cabin. *International Journal of Railway Technology **4**, 3*, doi: 10.4203/ijrt.4.3.3. ©Saxe-Coburg Publications.

Lefebvre, A. H. (1989). *Atomization and Sprays, Taylor & Francis, Bristol PA.*

Lohse, D. (2020). Wie sich Tröpfchen und damit Viren nach dem Niesen oder Husten in Wolken ausbreiten. *Physik Journal **19**, Nr. 5* 18-19.

Morawska, L. (2006). Droplet fate in indoor environments, or can we prevent the spread of injection. *Indoor Air, 16(5),*335-347.

Ng, C.S., Chong, K.L., Yang, R., Li, M., Verzicco, R., Lohse, D. (2021). *Phys. Rev. Fluids **6**, 054303.*

Public Transit and COVID-19 Pandemic: Global Research and Best Practices. *American Public Transportation Association. Sam Schwartz Consulting, September 2020.*

Rail Industry Coronavirus Forum. RSSB. https://customer-portal.rssb.uk/ accessed April 2021.

Reitz, R. D., & Diwakar, R. (1987) Structure of High-Pressure Fuel Sprays. *SAE Paper 860469.*

Rosin, P., Rammler, E. (1933). Die Gesetze über die Feinheit von Kohlenpulver. *Journal of the Institute of Fuel 7,* 29-36.

Scharfman, B. E., Techet, A. H., Bush, J. W. M., Bourouiba, L. (2016). Visualization of Sneeze Ejecta: Steps of Fluid Fragmentation Leading to Respiratory droplets. *Exp. Fluids, 57:24,* doi 10.1007/s00348-015-2078-4.

Schmidt, D. P., Nouar, I., Senecal, P. K., Rutland, C. J., Martin, J. K., Reitz, R. D., & Hoffman J. A. (1999). Pressure-Swirl Atomization in the Near Field. *SAE Technical Paper Series, 1999-01-0496.*

Senecal, P. K. Schmidt, D. P., Nouar, L., Rutland, C. J., & Reitz, R. D. (1999). Modeling High Speed Viscous Liquid Sheet Atomization. *Int. J. Multiphase Flow, **25**,* 1073-97.

TRANSCOM/AMC (2020). Commercial Aircraft Cabin Aerosol Dispersion Tests, Final Report, NSRI, ZeteoTech, S3I.

User Guide StarCCM+, CD-adapco. (2014). Version 9.06.

Wang, H., Lin M., & Chen, Y. (2014). Performance evaluation of air distribution systems in three different China railway high-speed train using numerical simulations. *Building Simulation,* 629–63.

Wells, W. F., (1934). On air-borne infection: Study II. Droplets and droplet nuclei, *Am. J. Epidemiol. **20***, 611.

Yan, Y., Li, X., Yang, L., Yan, P., & Tu, J. (2020). Evaluation of cough-jet effects on the transport characteristics of respiratory-induced contaminants in airline passengers' local environments. *Building and Environment 183 107206.*

Yang, S., Lee, G. W. M., Chen, C. M., Wu, C. C., & Yu, K.P. (2007). The size and concentration of droplets generated by coughing in human subjects. *Journal of Aerosol Medicine. **20**(4), 484-494.*

Yang, W., & Marr, L. C. (2011). Dynamics of Airborne Influenza A Viruses Indoors and Dependence on Humidity. *PLoS ONE 6(6).*

Zhang, L., & Li, Y. G. (2012). Dispersion of coughed droplets in a fully-occupied high-speed rail cabin. *Building and Environment **47,*** 58-66.